Impacts of the Boreal Summer Intraseasonal Oscillation (BSISO) on Precipitation Extremes in Indonesia

Fadhlil R. Muhammad[1] and Sandro W. Lubis[2]

[1]School of Geography, Earth, and Atmospheric Sciences, University of Melbourne, Melbourne, Australia

[2]Rice University, Houston, Texas, USA

ABSTRACT

The relationship between boreal summer intraseasonal oscillation (BSISO) and precipitation extremes over Indonesia is investigated using observational datasets from 30 years (1987 – 2016) of rain gauge measurements and the gridded Asian Precipitation–Highly Resolved Observational Data Integration Toward Evaluation of Water Resources (APHRODITE) from 1998 – 2015. The results indicate that the frequency of extreme precipitation events in Indonesia (defined as total precipitation above the 95th percentile) during extended boreal summer (May-August) is significantly modulated by BSISO, especially over the western and northern regions. Under the influences of BSISO1, the probability of the precipitation extremes over Sumatra and Borneo increases by 20 - 120% during phases 1 to 3, and approximately 50 – 80% over the eastern part of Borneo and Sulawesi during phase 4. Under the BSISO2, the probability of the extremes increases up to 40% over Sumatra during phases 1 to 2 and up to 140% over the Borneo and Sulawesi during phases 2 - 3. The increase in the probability of extreme summer precipitation is associated with enhanced large-scale moisture flux convergence and upward moisture transport induced by BSISO active phases. These results may provide valuable information for medium-to-extended-range prediction of summer precipitation extremes in Indonesia.

Keywords BSISO, precipitation extreme, tropical precipitation, equator, maritime continent

1. Introduction

Intraseasonal oscillation exhibits pronounced impacts on tropical weather and climate (Wang and Xie, 1997; Lee et al., 2013; Hsu et al., 2016, Ren et al., 2018; Chen and Wang, 2021; Olaguera et al., 2021). In particular, boreal summer intraseasonal oscillation (BSISO) plays a dominant role in controlling climate variability over the Indo-Pacific warm pool region during boreal summer (Wang and Xie, 1997, Hsu et al., 2016, Olaguera et al., 2021). Unlike Madden-Julian Oscillation (MJO), BSISO has a more complex structure and characteristics due to its interaction with other tropical mode variability such as equatorial eastward, off-equatorial westward, and northward propagating low-frequency modes (Lee et al., 2013; Ren et al., 2018; Chen and Wang, 2021).

BSISO consists of two types of intraseasonal oscillation modes: the 30 – 60 days oscillation period (BSISO1) and the 10 – 20 days oscillation period (BSISO2) (Lee et al., 2013; Ren et al., 2018; Chen and Wang, 2021). The BSISO1 is characterized by the northward propagation of the convective anomalies, starting over the Indian Ocean with a period of 30 – 60 days. In general, the propagation feature of the BSISO1 is similar to the boreal summer MJO, except it is more asymmetric and extended more northward/northeastward rather than eastward (Annamalai and Sperber, 2004; Muhammad et al., 2021a; Waliser et al., 2009; Lee et al., 2013). Previous studies showed that the northward propagation of BSISO1 is associated with the vertical easterly shear and moisture advection, which produces the barotropic vorticity to the north of convection (Jiang et al., 2004, Lee et al., 2013). More recently, Yang et al., (2020) found that the meridional gradient of sea surface temperature anomalies can affect the northward propagation of BSISO.

The BSISO2 is charactherized by northward/northwestward propagation of large-scale convective pattern with a period of 10 – 20 days (Lee et al., 2013). The characteristics of the BSISO2 are similar to the rapid annual cycle of the Asian Summer Monsoon (ASM) (LinHo and Wang, 2002). The BSISO2 emerges from the interaction of the eastward Kelvin-Rossby wave packet from the Indian Ocean with the northern hemisphere summer monsoon region (Wang and Xie, 1997). A more recent study using a fully-coupled earth system model indicates that the mean state of the vertical shear in the south Asian Monsoon region plays an important role in the northward propagation of BSISO2 (Yang et al., 2019).

Previous studies have found that BSISO has a major role in organizing tropical precipitation over the Asian Monsoon region during boreal summer (Chen et al., 2015; Lee et al., 2017; Mao et al., 2010; Mao and Wu, 2006; Ren et al., 2018; Zhu et al., 2003). For example, BSISO increases the extreme precipitation probability (95th percentile) over the Philippines by around 80% (Olaguera et al., 2021). In Indonesia, BSISO causes floods and extreme precipitation events over North Sumatra (Faqih and Nurussyifa, 2017), with a high occurrence of extremes during phases 1 – 3 of BSISO1 and phases 1 and 2 of BSISO2. Although these studies have shown the importance of the BSISO in modulating summer precipitation variability over those regions, a comprehensive study of the impacts of BSISO on precipitation extremes over the whole Maritime Continent remains elusive. This study aims to investigate the influence of BSISO on precipitation variability and extreme precipitation (during the extended boreal summer from May to August) over the Maritime Continent using rain gauge data from the local meteorological stations and the gridded Asian Precipitation–Highly Resolved Observational Data Integration Toward Evaluation of Water Resources (APHRODITE). Specifically, we would like to address the following questions:

1. What are the effects of the BSISO on intraseasonal precipitation variability and precipitation extremes during extended boreal summer in Indonesia?
2. What are the underlying physical processes for the modulation of BSISO on precipitation extremes?

2. Data and Methods

We use 30-year daily rain-gauge data from 63 meteorological stations in Indonesia from 1987 to 2016 as collected and compiled by the Indonesian Meteorology, Climatology, and Geophysics Agency (BMKG). The location of the stations can be seen in Figure 1. For data quality, we omit precipitation data with more than 30% of missing values for the analysis, resulting in a total of 60 stations used for the analysis (see Table S1 for details). We also used Asian Precipitation – Highly Resolved Observational Data Integration

Towards Evaluation of Water Resources (APHRODITE) (Yatagai et al., 2012) between 1998 and 2015. The APHRODITE data is produced using daily interpolated precipitation observation data from around the world, with a spatial resolution of 0.25 x 0. 25°. The dataset is interpolated by considering the effect of topography, thereby improving the representation of precipitation variation over the mountainous regions (Schaake, 2004).

The BSISO event is defined using the Real-time Multivariate BSISO index (RMM) (Lee et al., 2013). The BSISO RMM is similar to Madden-Julian Oscillation (MJO) but with different empirical orthogonal functions (EOF) configuration. The BSISO RMM index is generated by taking the multivariate EOF from outgoing longwave radiation (OLR) and zonal wind at 850 hPa over the region 10°S–40°N and 40°–160°E. The first two leading principal components (PC1 and PC2) are then defined as BSISO1, while the second pair is defined as BSISO2 (PC3 and PC4). If the amplitude of the PC (e.g., $\sqrt{(PC1^2 + PC2^2)}$) is more than 1, it is defined as a strong BSISO event.

To investigate the influence of BSISO on precipitation extremes, we first calculate the number of precipitation events that occurred beyond the 95th percentile thresholds for each grid point. Then, we calculate the changes in the probability of extreme precipitation for May-August precipitation probability as follows (Hsu et al., 2016; Ren and Ren, 2017):

$$\Delta P = \frac{P_{BSISO} - P_{ALL}}{P_{ALL}} \times 100\%, \qquad (1)$$

Where ΔP is the change of the probability of extreme precipitation, P_{BSISO} is the probability of precipitation exceeding the threshold (95th percentile) during each phase of the BSISO event, and P_{ALL} is the same as P_{BSISO}, but for all non-zero precipitation days during the season. The identified extreme precipitation thresholds for each region in Indonesia are shown in Figure 1b (see Table S1 for each station's extreme precipitation threshold).

To analyze the dynamical processes for modulations of BSISO on precipitation extremes, we use the OLR dataset from NOAA/NESDIS (Liebmann and Smith, 1996) and zonal, meridional, and vertical wind, relative humidity, and air temperature from the

NCEP/DOE Reanalysis 2 (Kanamitsu et al., 2002). We then calculate the moisture flux convergence (MFC) associated with the BSISO event (Banacos and Schultz, 2005):

$$MFC = \underbrace{\left[-u\frac{\partial q}{\partial x} - v\frac{\partial q}{\partial y}\right]}_{convegence\ term} + \underbrace{\left[-q\left(\frac{\partial u}{\partial x} + \frac{\partial v}{\partial y}\right)\right]}_{advection\ term}, \quad (2)$$

where u is zonal wind, v is meridional wind, and q is specific humidity. The vertically integrated MFC in the troposphere can be further decomposed into two terms:

$$Conv.\,MFC = \frac{1}{g}\int_{1000\,hPa}^{100\,hPa}\left[-u\frac{\partial q}{\partial x} - v\frac{\partial q}{\partial y}\right]dp, \quad (3)$$

$$Adv.\,MFC = \frac{1}{g}\int_{1000\,hPa}^{100\,hPa}\left[-q\left(\frac{\partial u}{\partial x} + \frac{\partial v}{\partial y}\right)\right]dp, \quad (4)$$

where g is the gravity (9.81 ms^{-2}). The convergence MFC term represents the sum of horizontal convergence of moisture from 1000 hPa to 100 hPa, whereas the advection MFC term represents the sum of horizontal advection of moisture.

Using these datasets, we generate composite anomalies for each phase of the BSISO. The anomalies are calculated as the deviation from the daily climatology. The anomalies are then bandpass filtered for a period of 20 – 90 days for BSISO1 and 5 – 70 days for BSISO2 according to the power spectra of BSISO1 and BSISO2 (Lee et al., 2013). The large bandpass filter range for BSISO2 is due to the EOF3, which has a longer period of around 60-70 days (Lee et al., 2013). Since the EOF3 of the BSISO has a large variance over the western part of Indonesia (Lee et al., 2013), we decided to accommodate this by taking a more extensive period range than usual (i.e., 5 – 70 days as opposed to 10 – 20 days).

A significant test for both the probability and composites analysis is done by using a bootstrap method (Wilks, 2006). We start with generating 1000 synthetic composites for each phase of the BSISO, then derive the confidence level by sorting the composites in order to find the percentiles corresponding to the confidence level (i.e., 97.5^{th} and 2.5^{th} percentiles for a 95% confidence level).

3. Results and Discussions

3.1 Life-Cycle of BSISO

We begin our analysis by examining the propagation features of BSISO during its life cycle. Figures 2 and 3 show the life cycle composites of OLR and horizontal wind anomalies at 850-hPa on eight phases of BSISO1 and BSISO2, respectively. General characteristics of BSISO1 propagation (Figure 2) are as follow: The convection anomaly appears over the Indian Ocean during phase 1, with a significant portion of the enhanced convection reaching the Sumatra island and west of Borneo island. The enhanced convection and associated low-level cyclonic anomalies propagate further eastward over the Indian ocean and reach some parts of the Borneo island during phase 2 (Fig. 2b). During this phase, suppressed convection and low-level anticyclonic anomalies are located over the north of the Philippines. During phases 3 and 4, the enhanced convection migrates further eastward and northward (Figs. 2c-d), covering most of the eastern part of Borneo, the northern part of Sulawesi, and some of the Papua islands. During phases 5 – 8, general propagation features of BSISO1 are similar to those observed during phases 1 – 4 but with opposite signs (Fig. 2e – h). For example, suppressed convection is observed in most Indonesian regions during phase 7 instead of enhanced convection during phase 3.

The life-cycle composite of BSISO2 shows different propagation features compared to BSISO1. The enhanced convection begins over the Indian Ocean and the Philippine Sea during phase 1 (Fig. 3a). At this stage, twin cyclonic anomalies are observed over these regions. The convective anomalies over the Indian Ocean become stronger in phase 2 (Fig. 3b) and propagate northward to the north of the Philippine sea in phase 3 (Fig. 3c). During phase 4, the enhanced convection accompanied by strong anticyclonic and westerly wind anomalies migrates further northeastward to the Luzon strait and Western North Pacific-East Asian regions (Fig 3d). The propagation features of BSISO2 during phases 5-8 resemble those observed during phases 1 – 4 of BSISO2, but with opposite signs (Fig. 3e – g and Fig. 3a – d).

The regional differences in the propagation features of BSISO1 and BSISO2 discussed above suggest that the spatial variations should be considered when investigating the regional impacts of BSISO on extreme precipitation over Indonesia. In the next sections, we investigate whether the active convection induced by BSISO significantly influences intraseasonal precipitation variability and extreme precipitation events during summer over specific regions in Indonesia.

3.2 Influence of BSISO on Intraseasonal Precipitation Variability

Figure 4 shows the composite map of precipitation anomalies during different active phases of BSISO1 calculated from the rain gauge and APHRODITE datasets. During phase 1, daily precipitation increases by up to 3 mm/day in APHRODITE (or about 1 – 3 mm/day from the rain gauges) over most Sumatra and Borneo islands, Sulawesi, and the western part of Papua island (Fig. 4a), equivalent to approximately 30 – 100% relative to the mean seasonal precipitation (i.e., 3 – 9 mm/day). During phase 2 (Fig. 4b), the increase in precipitation is generally higher than those during phase 1 and extends towards the central region of Indonesia, with the strongest impact observed over the Sumatra island and Borneo island. During phase 3, the increase in precipitation is observed mostly over Sumatra, Central Java, Borneo, and Sulawesi (Fig. 4c). The increase in precipitation further moves to the northern and eastern parts of Indonesia during phase 4 (Fig. 4d), consistent with the northeastward migration of the BSISO1-associated convection (Fig. 2d). This increase in precipitation over the southern regions may be due to the mixed influence with the boreal summer MJO, as it tends to occur in conjunction with BSISO (Lee et al., 2013). Overall, these results are consistent with the propagation of the convective center associated with BSISO1 (Fig. 2). During phases 5 – 8 (Fig. 4e – h), the suppressed phases of BSISO decrease the precipitation over the majority of the Indonesian regions by approximately 1-3 mm/day in APHRODITE or 1-5 mm/day in rain gauges. Particularly, during phases 6 and 7 (Fig 4f and 4g), Sumatra, Borneo, and Sulawesi islands experience the greatest influences from the BSISO-associated suppressed convection.

During active phases of BSISO2, the largest increase in precipitation is observed in phases 2 – 3 (Fig. 5). During phase 1, northern Sumatra and Borneo experience a small increase in precipitation by up to 1 mm/day in the APHRODITE and up to 2 mm/day for the rain-gauges (Fig 5a). A significant impact of the BSISO on precipitation anomaly is observed during phase 2 due to the strengthening of BSISO-associated convection (Fig 3b). During this phase, most regions in Borneo, Sumatra, Sulawesi, and western Java islands experience an increase in precipitation by more than 3 mm/day in the APHRODITE and the rain-gauge data. During phase 3, BSISO increases the precipitation over the northwest of Sumatra, Sulawesi, Borneo, and a small part of the western Java island. We also note that during phase 3 of BSISO2 (Fig. 5c), a decrease in precipitation is also observed over some regions in Sumatra. Such a decrease might be related to the South China sea monsoon, which shows a negative relationship with precipitation over Sumatra (Zhang et al., 2018). A previous study showed that the South China Sea monsoon onset is closely associated with phases 2 – 4 of BSISO2 (Lee et al., 2013) and thus, may interfere with the precipitation over the region at the time of active monsoon. Finally, during phases 4 through 8, BSISO2 mainly decreases the precipitation over most regions in Indonesia, particularly over Sumatra during phase 5, by up to 3 mm/day in the APHRODITE data or up to 6 mm/day from the rain-gauges (Figs. 5d-h).

3.3 Influence of BSISO on Extreme Precipitation

Figure 6 shows the composites of percentage change in the probability of precipitation extremes during BSISO1 phases 1–8. In general, we can see that the probability of the precipitation extremes increases by up to 20 - 120% in APHRODITE (by 25-50% in rain gauge data) during phases 1 to 3 over Sumatra and Borneo (relative to the May-August precipitation probability) (Figs. 6a-c), and approximately 50 – 80% (by 25-50% in rain gauge data) over the eastern part of Borneo and Sulawesi during phase 4 (Fig. 6d). During phases 5 through 8, the probabilities of precipitation extremes decrease over most of the Indonesian regions (Figs. 6e-h). In particular, a decrease in precipitation over the western part of Indonesia, such as Sumatra, Borneo, and the western part of Java, reaches up to 20 – 70% for the APHRODITE or around 50% for the rain-gauges in phase 5. During phases 6 and 7, a decrease in the probability of precipitation extremes over Sumatra, Borneo, and Sulawesi is up to 70% for the APHRODITE or around 50% from the rain-gauges, while during phase 8, the decrease by up to 50 – 80% for the APHRODITE or around 50% for the rain-gauges cover most regions in Borneo.

The percentage changes in the probability of precipitation extremes the phases 1–8 of BSISO2 are shown in Figure 7. In general, the influences of BSISO2 on extreme precipitation are significant over the western and central parts of Indonesia. In particular, the probability of the extremes significantly increases by up to 40% over Sumatra during phases 1 to 2 (Figs. 7a-b) and by up to 140% over the Borneo and Sulawesi during phases 2 – 3 (Figs. 7b-c). During phases 4 to 8, the BSISO2 significantly decreases the probability of precipitation extremes in the majority of the Indonesian regions (Figs. 7d,h). In the APHRODITE data, the strongest decrease in extreme probability is observed during phases 6 and 8 (Fig. 7d and h) by approximately 60% over Sumatra and Papua. It is also interesting to note that the impact of BSISO2 phases 4 – 8 on extreme precipitation is relatively weaker than those during BSISO1 phases 5 – 8. This is consistent with the nature of convective activity associated with BSISO2, which shifts further northward during those phases (i.e., moving to the Philippine Sea and Indochina), resulting in a weaker influence on precipitation variability over precipitation in Indonesia.

To summarize the mean of regional impacts of different phases and types of BSISO on precipitation extremes in Indonesia, we also calculate the areal-averaged changes in extreme precipitation probability associated with BSISO (Figure 8). We divide Indonesia into four regions, representing the western, northern, southern, and eastern parts of Indonesia (Fig. 1a). The western region includes Padang city in the west Sumatra, the eastern region includes Manokwari in the West Papua, the southern region includes the capital city of Jakarta, and the northern region includes the proposed new capital city of Indonesia, East Kalimantan.

Over the western part of Indonesia (represented by the region/box "A" in the figure), the strongest impacts of BSISO1 (BSISO2) are observed during phases 2 – 3 (phases 1-2) (Fig 8a). The overall impacts of BSISO1 are stronger than those during BSISO2. This result is consistent with the characteristics of BSISO-induced large-scale convection over the Maritime Continent (Figs. 2 and 3). Furthermore, the impact of BSISO over East Kalimantan, the northern region of Indonesia (represented by "B"), is the strongest compared to the other regions in Indonesia (Fig. 8b). Increases in extreme precipitation probability by approximately 100 - 120% are observed during phases 2-4 of BSISO1 (Fig. 8b). On the other hand, the strongest impacts of BSISO2 are observed during phase 2 by up to 120%. Compared to the western or northern regions, the impacts of BSISO over the eastern part of Indonesia (represented by “C”) are relatively weak (Fig 8c). In this region, BSISO1 increases the extreme precipitation probability by approximately 50% and 80% during phases 1 and 4, while BSISO2 increases the extreme precipitation probability by approximately 40% and 60% during phases 5 and 7, respectively (Fig 8c). Finally, the influences of BSISO in the southern region of Indonesia (represented by the region “D”) are relatively weaker, with significant influences during phase 3 of BSISO1 and during phases 2 and 3 of BSISO2 (Fig. 8d), consistent with weaker convective activity associated with BSISO1 and BSISO2 over the region.

3.4 Dynamical links between BSISO and precipitation extremes

Overall, our results show that enhanced convection associated with BSISO leads to an increase in precipitation and extreme probability in Indonesia during the boreal summer, particularly over the western and northern parts of Indonesia. To better understand the physical processes associated with the BSISO modulations on precipitation extremes, we examine moisture flux convergence (MFC) and vertical moisture advection during the events, which have been considered to be important factors of extreme precipitation during BSISO (Hsu et al., 2016; Ren et al., 2018). We only focus on the active phases of BSISO (phases 1 – 4) that drive an increase in the probability of precipitation extremes in Indonesia. Similar processes responsible for the decreased probability during phases 5-8 can be found in the supplement (see Figs. S1 and S2).

Figure 9 shows the composites of the convergence and advection terms of MFC anomalies (see Eq. 3 and 4) for each convective phase of BSISO1. It can be seen that the magnitude of the convergence term is approximately three times stronger than the advection term. This indicates that the moisture convergence is the main driver of the extreme precipitation associated with BSISO, consistent with Hsu et al., (2016). During phases, 1 to 3 of BSISO1, the convergence term of MFC is observed over most regions of Indonesia. The convergence term is collocated with cyclonic wind anomalies over the region and, therefore, consistent with increases in precipitation and extreme precipitation probability over the regions (Fig. 4 and Fig. 6). In particular, when the highest impact is observed over Sumatra, Borneo and Sulawesi during phase 2 of BSISO1 (Fig. 6b), the enhanced convergence of moisture flux is also observed over these regions. These results suggest that the enhanced large-scale moisture flux convergence (i.e., positive MFC) induced by BSISO1 is closely related to an increase in precipitation and extreme probability. On the other hand, the decreases in precipitation and extreme precipitation probability over the regions are associated with suppressed convergence of moisture flux due to the anomalous anticyclone (see Fig. S1 in the supplement).

Similarly, the increase of extreme precipitation induced by BSISO2 is largely driven by moisture flux convergence. During phase 1 of BSISO2, a moisture convergence was observed over the northwestern coast of Sumatra, collocated with the anomalous cyclone at the 850-hPa (Fig. 10a). During this phase, extreme precipitation probability is observed over the western part of Indonesia (Figs. 5 and 7), consistent with the enhanced convergence and advection MFC shown in Figure 10a. Moreover, the moisture convergence and advection strengthen during phase 2 of BSISO2 (Figure 10b), which results in increases in precipitation and extreme precipitation probability over most of the western and northern parts of Indonesia (Figs. 5 and 7). Overall, the probability of extreme precipitation increases (decreases) is consistent with the progression of the anomalous convergence (divergence) of moisture flux (Figs. 9-10).

To further elucidate the role of large-scale convection induced by BSISO on extreme precipitation, we also analyze the vertical advection of moisture. The vertical moisture advection has also been shown to play an important role in explaining the enhanced (suppressed) upward (downward) motion of moist air over the region(Muhammad et al., 2021a, 2021b; Ren et al., 2018). The vertical moisture advection is defined as follows:

$$Vert.\ Moist.\ Adv. = -\omega\frac{dq}{dp}. \qquad (5)$$

During phase 1 of BSISO1, upward moisture advection intensifies between 925 – 300 hPa over 75° – 105° E (Fig. 11a). This upward advection anomaly is collocated with the BSISO-associated enhanced convection and MFC (Fig. 2a and 9a). As the BSISO1 moves northeastward and influences more Indonesian regions, the enhanced upward moisture advection is also observed over the affected region (Fig. 11(b) – (d)). A similar result is also found for BSISO2, albeit in a weaker magnitude. Phase 1 of BSISO2 shows an enhanced upward moisture advection at around 925 – 400 hPa over 75° – 120° E (Fig. 11e), consistent with the observed increase in extreme precipitation probability (Fig. 7a). During phase 2, the vertical moisture advection is also the strongest. This result is consistent with enhanced MFC (Fig. 9b) and the changes in precipitation anomaly and extreme precipitation probability (Fig. 4b and 6b), the strongest during phase 2 of BSISO2. At this stage, a strong deep upward moisture advection is observed at around 925 – 250 hPa over 75° – 120° E (Fig. 11b), collocated with the region that experiences an increase in precipitation (Fig. 7b).

In summary, both moisture convergence and upward advection of moisture play an essential role in explaining the regional-scale differences in the impacts of BSISO on extreme precipitation in Indonesia. This result suggests that during a BSISO active phase, the combination of moisture convergence and upward moisture advection due to BSISO favor the development of deep convective clouds over the affected region, resulting in extreme precipitation. This result is consistent with a previous study, which demonstrates that a deep upward moisture advection supports the development of deep convection when combined with moisture convergence (e.g., Benedict and Randall, 2007).

4. Concluding remarks

In this study, we investigated the influence of BSISO on the probabilities and spatial distributions of precipitation extremes over Indonesia during extended boreal summer (May to August) using observational data from local rain-gauge measurements from 1987 to 2016 and the gridded precipitation dataset of APHRODITE from 1988 to 2015. Our major findings are summarized as follows:

- BSISO significantly influences intraseasonal precipitation variability and extreme precipitation in Indonesia during extended boreal summer (May to August).
- BSISO1 increases the probabilities of extreme precipitation over Sumatra and Borneo by 20 - 120% during phases 1 to 3 and approximately 50 – 80% over the eastern part of Borneo and Sulawesi during phase 4.

- BSISO2 increases the probability of precipitation extremes by more than 40% over Sumatra during phases 1 to 2 and up to 140% over the Borneo and Sulawesi during phases 2 - 3.
- The increase in the probability of extreme-precipitation events is associated with enhanced horizontal moisture convergence and vertical moisture advection induced by BSISO active phases.

Our results indicate a significant regional-scale influence of the BSISO on summer extreme precipitation events in Indonesia. However, it is possible that other atmospheric processes can influence precipitation extremes in Indonesia during boreal summer through their interaction with BSISO. For example, the South China Sea monsoon onset (Kajikawa and Wang, 2012; Wang et al., 2004; Zhang et al., 2018) has been shown to be related to BSISO (Lee et al., 2013) and may interact with the precipitation over the western part of Indonesia. On the other hand, the onset of the Indian Summer monsoon, which has a negative correlation with precipitation over the central and eastern part of Indonesia (Karmakar and Misra, 2019; Klingaman et al., 2008; Kripalani and Kulkarni, 1997), can interfere the modulation of BSISO on precipitation over the regions (Lee et al., 2013). Furthermore, the effects of diurnal cycle, topography and large-scale atmospheric systems such as convectively coupled equatorial waves (CCEWs) may also interact with BSISO and influence the regional impacts of BSISO on extreme precipitation (Hsu and Lee, 2005; Wu and Hsu, 2009; Lubis and Jacobi, 2015; Lubis and Respati, 2021). Therefore, understanding the interaction between BSISO and other low-and-high frequency variabilities and the resulting impacts on precipitation remains to be further studied.

The results of this study could be leveraged for developing a skillful subseasonal forecast of precipitation extremes over some regions in Indonesia during boreal summer. Improved forecasting of precipitation extremes over Indonesia could provide valuable information to farmers, water resource managers, and other stakeholders for disaster management.

Acknowledgments

We are grateful for the gridded precipitation data from the APHRODITE (http://aphrodite.st.hirosaki-u.ac.jp/products.html) and the rain-gauge dataset from BMKG (http://dataonline.bmkg.go.id/home). All authors have contributed equally.

Conflict of interest

The authors report that they have no conflict of interest.

References

Annamalai, H., Sperber, K.R., 2004. Regional Heat Sources and the Active and Break Phases of Boreal Summer Intraseasonal (30-50 Day) Variability. Journal of the Atmospheric Sciences 38.

Banacos, P.C., Schultz, D.M., 2005. The use of moisture flux convergence in forecasting convective initiation: Historical and operational perspectives. Weather and Forecasting 20, 351–366. https://doi.org/10.1175/WAF858.1

Benedict, J.J., Randall, D. a., 2007. Observed Characteristics of the MJO Relative to Maximum Rainfall. Journal of the Atmospheric Sciences 64, 2332–2354. https://doi.org/10.1175/JAS3968.1

Chen, J., Wen, Z., Wu, R., Chen, Z., Zhao, P., 2015. Influences of northward propagating 25–90-day and quasi-biweekly oscillations on eastern China summer rainfall. Climate Dynamics 45, 105–124. https://doi.org/10.1007/s00382-014-2334-y

Faqih, A., Nurussyifa, D., 2017. Intraseasonal rainfall variability in North Sumatra and its relationship with Boreal Summer Intraseasonal Oscillation (BSISO). IOP Conference Series: Earth and Environmental Science 54. https://doi.org/10.1088/1742-6596/755/1/011001

Hsu, H.-H., Lee, M.-Y., 2005. Topographic effects on the eastward propagation and initiation of the Madden--Julian oscillation. Journal of Climate 18, 795–809. https://doi.org/https://doi.org/10.1175/JCLI-3292.1

Hsu, P.C., Lee, J.Y., Ha, K.J., 2016. Influence of boreal summer intraseasonal oscillation on rainfall extremes in southern China. International Journal of Climatology 36, 1403–1412. https://doi.org/10.1002/joc.4433

Jiang, X., Li, T., Wang, B., 2004. Structures and mechanisms of the northward propagating boreal summer intraseasonal oscillation. Journal of Climate 17, 1022–1039. https://doi.org/10.1175/JCLI3861.1

Kajikawa, Y., Wang, B., 2012. Interdecadal change of the South China Sea summer monsoon onset. Journal of Climate 25, 3207–3218. https://doi.org/10.1175/JCLI-D-11-00207.1

Kanamitsu, M., Ebisuzaki, W., Woollen, J., Yang, S.-K., Hnilo, J.J., Fiorino, M., Potter, G.L., 2002. NCEP-DOE AMIP-II Renalalysys (R-2). Bull Am Meteorol Soc 83, 1631–1643. https://doi.org/10.1175/BAMS-83-11

Karmakar, N., Misra, V., 2019. The Relation of Intraseasonal Variations With Local Onset and Demise of the Indian Summer Monsoon. Journal of Geophysical Research: Atmospheres 124, 2483–2506. https://doi.org/10.1029/2018JD029642

Klingaman, N.P., Weller, H., Slingo, J.M., Inness, P.M., 2008. The intraseasonal variability of the Indian Summer monsoon using TMI sea surface temperatures and ECMWF reanalysis. Journal of Climate 21, 2519–2539. https://doi.org/10.1175/2007JCLI1850.1

Kripalani, R.H., Kulkarni, A., 1997. Rainfall variability over Southeast Asia—connections with Indian monsoon and ENSO extremes: new perspectives. International Journal of Climatology: A Journal of the Royal Meteorological Society 17, 1155–1168. https://doi.org/https://doi.org/10.1002/(SICI)1097-0088(199709)17:11<1155::AID-JOC188>3.0.CO;2-B

Lee, J., Hsu, P., Moon, S., Ha, K., 2017. Influence of Boreal Summer Intraseasonal Oscillation on Korean Precipitation and its Long-Term Changes. Atmosphere (Basel) 27, 435–444.

Lee, J.Y., Wang, B., Wheeler, M.C., Fu, X., Waliser, D.E., Kang, I.S., 2013. Real-time multivariate indices for the boreal summer intraseasonal oscillation over the Asian summer monsoon region. Climate Dynamics 40, 493–509. https://doi.org/10.1007/s00382-012-1544-4

Liebmann, B., Smith, C.A., 1996. Description of a complete (interpolated) outgoing longwave radiation dataset. Bull Am Meteorol Soc 77, 1275–1277.

LinHo, L., Wang, B., 2002. The time-space structure of the Asian – Pacific Summer Monsoon : A fast annual cycle view. Journal of Climate 15, 2001–2019.

Lubis, S. W., and Jacobi, C., 2015. The Modulating Influence of Convectively Coupled Equatorial Waves (CCEWs) on the Variability of Tropical Precipitation. International Journal of Climatology 35, 7, 1465-1483.

Lubis, S. W., and Respati, M. R., 2020. Impacts of Convectively Coupled Equatorial Waves on Rainfall Extremes in Java, Indonesia. International Journal of Climatology 41, 4, 2418-2440.

Mao, J., Sun, Z., Wu, G., 2010. 20-50-day oscillation of summer Yangtze rainfall in response to intraseasonal variations in the subtropical high over the western North Pacific and South China Sea. Climate Dynamics 34, 747–761. https://doi.org/10.1007/s00382-009-0628-2

Mao, J., Wu, G., 2006. Intraseasonal variations of the Yangtze rainfall and its related atmospheric circulation features during the 1991 summer. Climate Dynamics 27, 815–830. https://doi.org/10.1007/s00382-006-0164-2

Muhammad, F.R., Lubis, S.W., Setiawan, S., 2021a. The influence of boreal summer Madden-Julian Oscillation on precipitation extremes in Indonesia. arXiv:2112.00001 [physics.ao-ph]. https://doi.org/10.13140/RG.2.2.35991.09127

Muhammad, F.R., Lubis, S.W., Setiawan, S., 2021b. Impacts of the Madden–Julian oscillation on precipitation extremes in Indonesia. International Journal of Climatology 41, 1970–1984. https://doi.org/10.1002/joc.6941

Olaguera, L.M.P., Manalo, J.A., Matsumoto, J., 2021. Influence of Boreal Summer Intraseasonal Oscillation on Rainfall Extremes in the Philippines. International Journal of Climatology 1–13. https://doi.org/10.1002/joc.7495

Ren, H., Ren, P., 2017. Impact of Madden–Julian Oscillation upon winter extreme rainfall in Southern China: Observations and predictability in CFSv2. Atmosphere (Basel) 8, 192–216. https://doi.org/10.3390/atmos8100192

Ren, P., Ren, H.L., Fu, J.X., Wu, J., Du, L., 2018. Impact of Boreal Summer Intraseasonal Oscillation on Rainfall Extremes in Southeastern China and its Predictability in CFSv2. Journal of Geophysical Research: Atmospheres 123, 4423–4442. https://doi.org/10.1029/2017JD028043

Schaake, J., 2004. Application of prism climatologies for hydrologic modeling and forecasting in the western U.S., in: Proceeding of the 18th Conference on Hydrology. American Meteorological Society, Seattle, WA, p. 5.3.

Waliser, D., Sperber, K., Hendon, H., Kim, D., Maloney, E., Wheeler, M., Weickmann, K., Zhang, C., Donner, L., Gottschalck, J., Higgins, W., Kang, I.S., Legler, D., Moncrieff, M., Schubert, S., Stern, W., Vitart, F., Wang, B., Wang, W., Woolnough, S., 2009. MJO simulation diagnostics. Journal of Climate 22, 3006–3030. https://doi.org/10.1175/2008JCLI2731.1

Wang, B., LinHo, Zhang, Y., Lu, M.M., 2004. Definition of South China Sea monsoon onset and commencement of the East Asian summer monsoon. Journal of Climate 17, 699–710. https://doi.org/10.1175/2932.1

Wang, B., Xie, X., 1997. A Model for the boreal summer intraseasonal oscillation. Journal of the Atmospheric Sciences 54, 72–86. https://doi.org/10.1175/1520-0469(1997)054<0072:AMFTBS>2.0.CO;2

Wilks, D.S., 2006. Statistical methods in the atmospheric sciences, 2nd ed. Elsevier, Cambridge, US. https://doi.org/10.1016/B978-008045405-4.00661-3

Wu, C.-H., Hsu, H.-H., 2009. Topographic influence on the MJO in the Maritime Continent. Journal of Climate 22, 5433–5448. https://doi.org/https://doi.org/10.1175/2009JCLI2825.1

Yang, Y.M., Wang, B., Lee, J.Y., 2019. Mechanisms of Northward Propagation of Boreal Summer Intraseasonal Oscillation Revealed by Climate Model Experiments. Geophysical Research Letters 46, 3417–3425. https://doi.org/10.1029/2018GL081612

Yatagai, A., Kamiguchi, K., Arakawa, O., Hamada, A., Yasutomi, N., Kitoh, A., 2012. APHRODITE: constructing a long-term daily gridded precipitation dataset for Asia based on a dense network of rain gauges. Bull Am Meteorol Soc 93, 1401–1415. https://doi.org/10.1175/BAMS-D-11-00122.1

Zhang, Y., Li, J., Xue, J., Feng, J., Wang, Q., Xu, Y., Wang, Y., Zheng, F., 2018. Impact of the South China sea summer monsoon on the Indian Ocean dipole. Journal of Climate 31, 6557–6573. https://doi.org/10.1175/JCLI-D-17-0815.1

Zhu, C., Nakazawa, T., Li, J., Chen, L., 2003. The 30-60 day intraseasonal oscillation over the western North Pacific Ocean and its impacts on summer flooding in China during 1998. Geophysical Research Letters 30, 2–6. https://doi.org/10.1029/2003GL017817

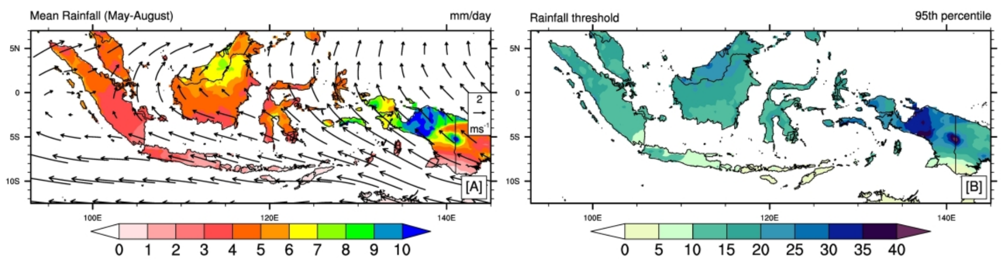

Figure 1. (a) May-August mean rainfall (color shading) from APHRODITE (1998 - 2015) superimposed with the 850-hPa wind (vector) from NCEP reanalysis (b) The 95th percentile of daily rainfall from May to August.

279x279mm (300 x 300 DPI)

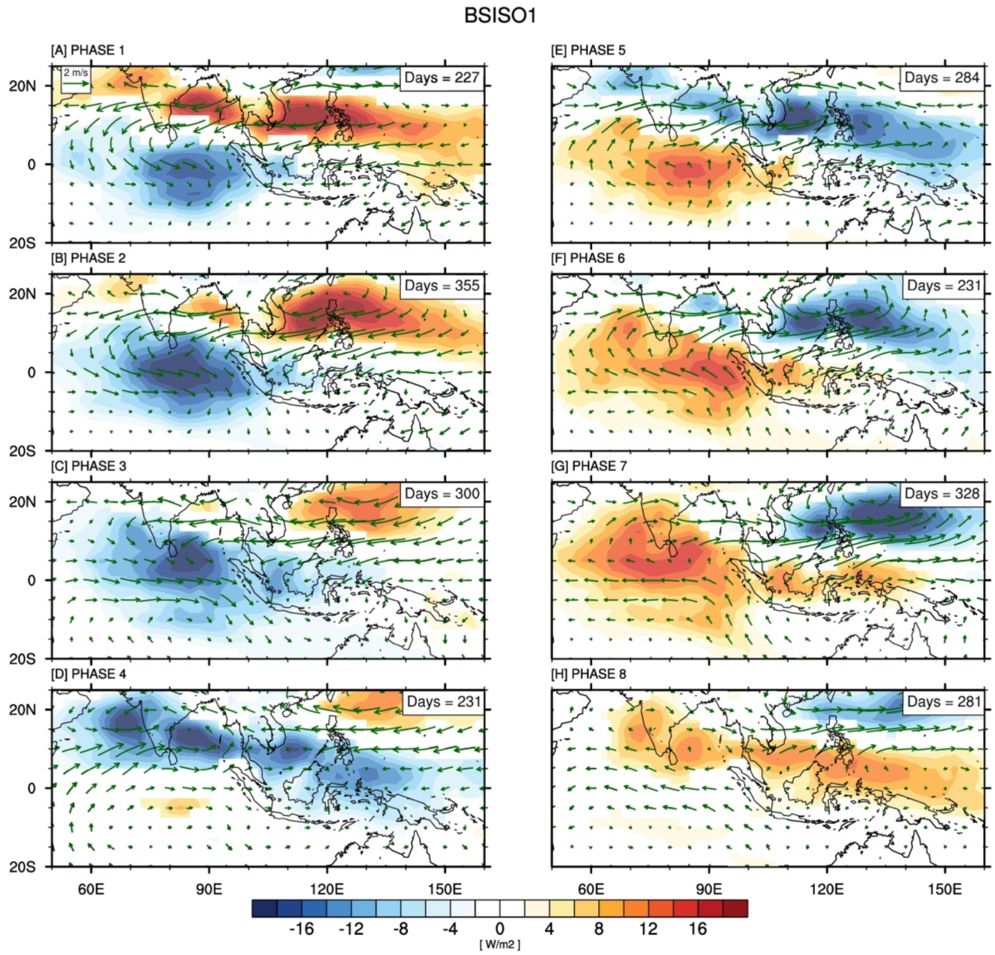

Figure 2. Life cycle composite of OLR anomaly (color shading) for each of eight phases of BSISO1 (a - h) overlaid by the 850 hPa wind anomaly (vector). Only values significant at the 95% confidence level are shaded for the OLR anomaly.

194x193mm (300 x 300 DPI)

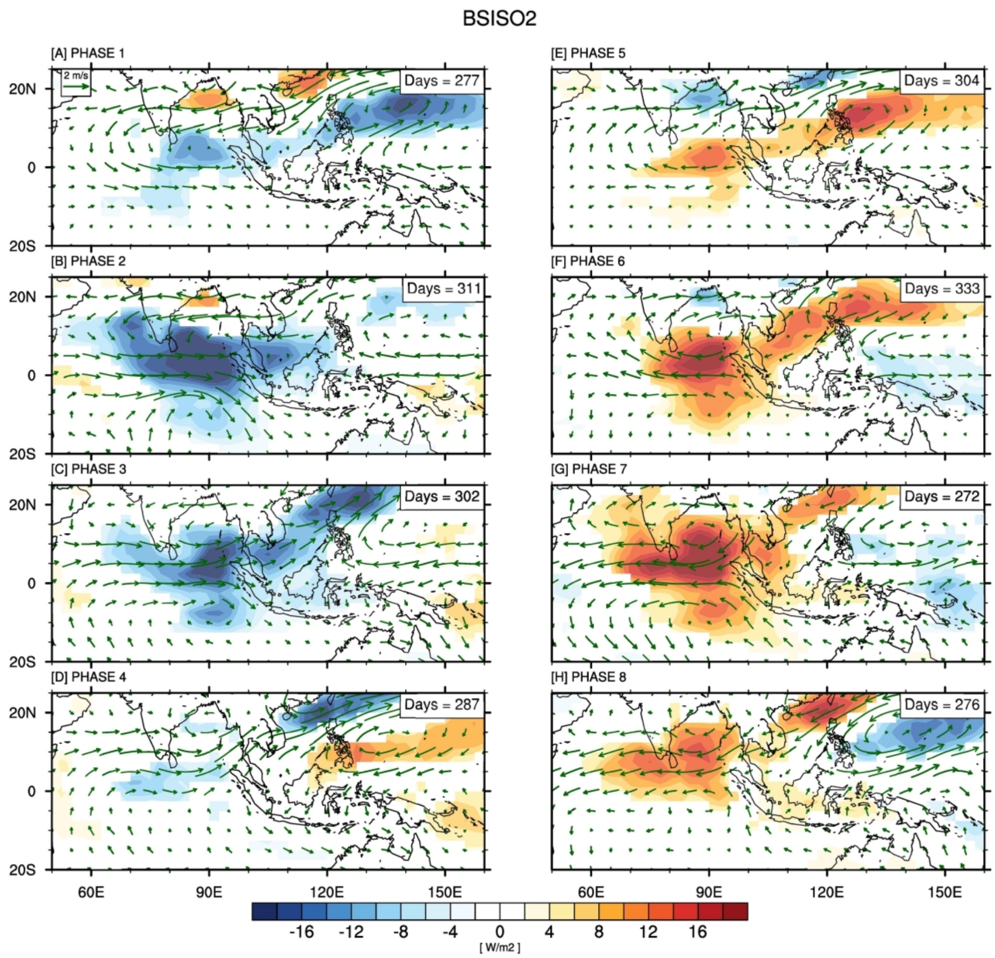

Figure 3. Same as Figure 2, but for each of eight phases of BSISO2.

194x193mm (300 x 300 DPI)

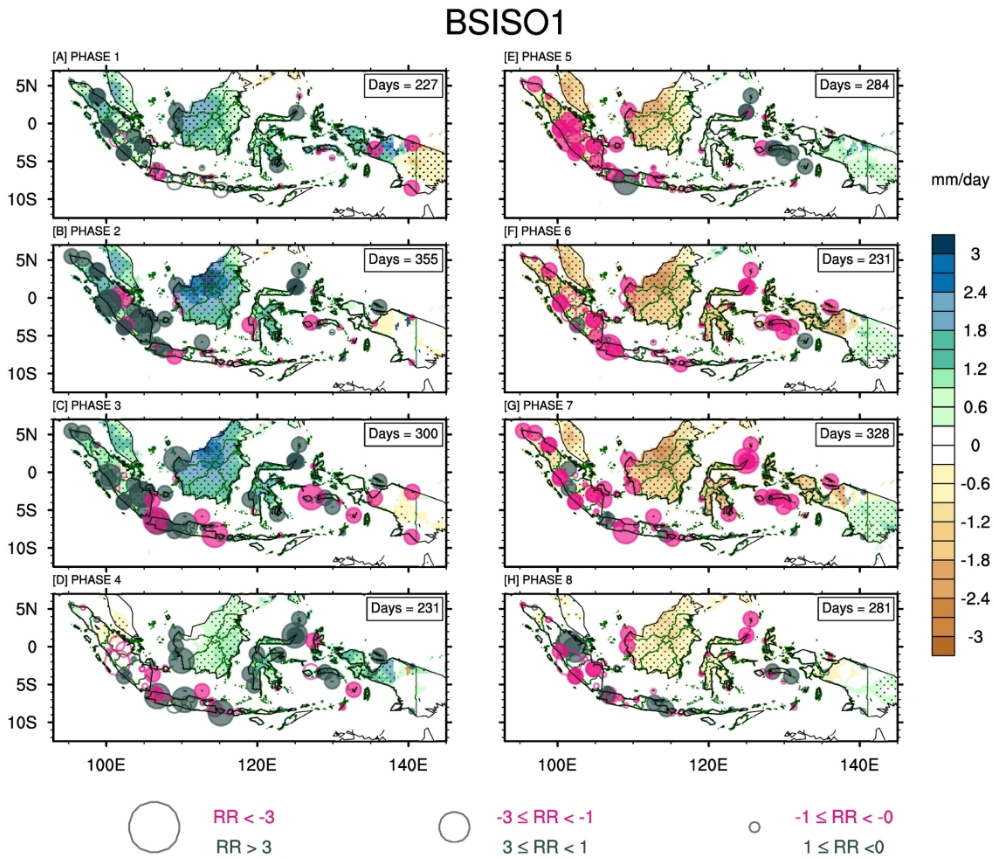

Figure 4. Life cycle composites of rainfall anomalies for each of eight phases of BSISO1. Color shading indicates rainfall anomalies obtained from APHRODITE, and red (gray) circles indicate positive (negative) anomalies obtained from rain-gauge data. Dots and filled circles indicate values that are statistically significant at a 95% level.

190x190mm (300 x 300 DPI)

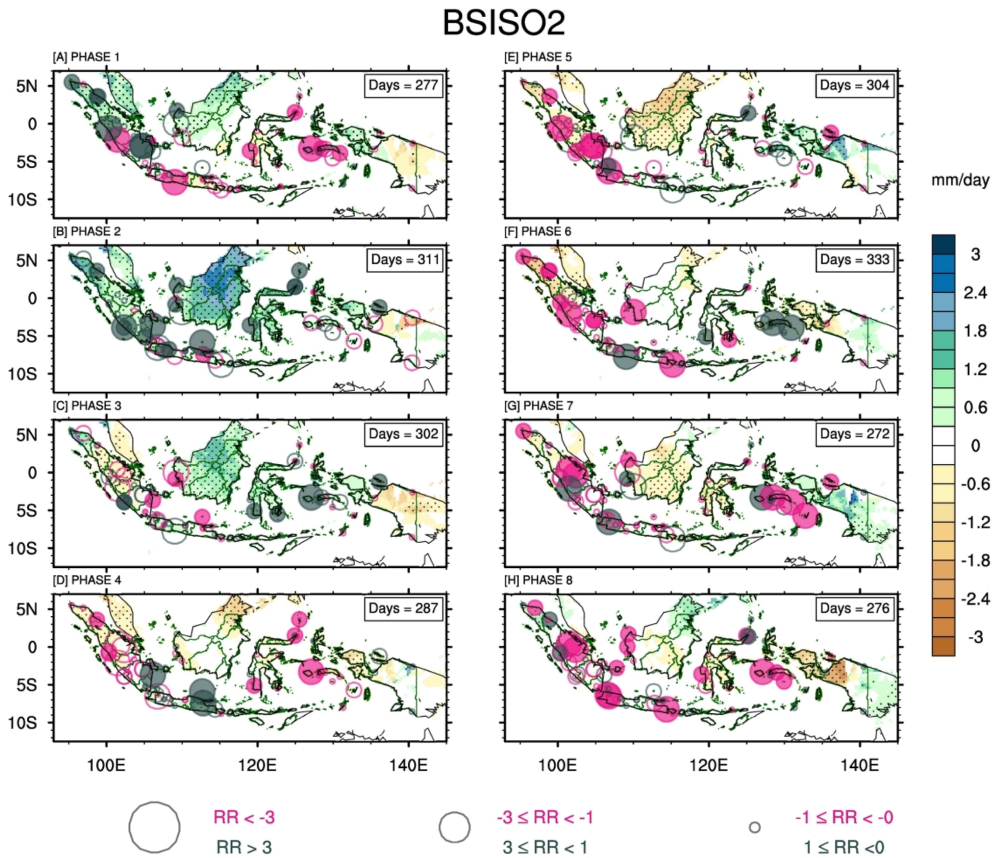

Figure 5. Same as Figure 4, but for BSISO2.

190x190mm (300 x 300 DPI)

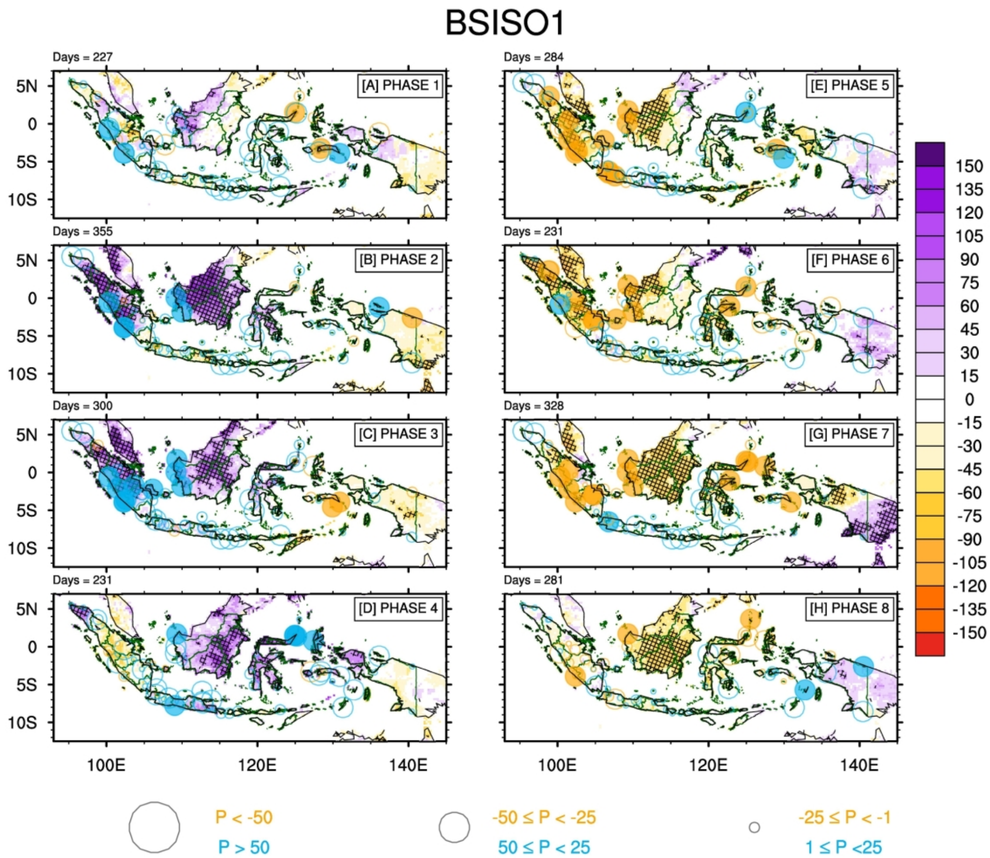

Figure 6. Percentage changes in the probability of rainfall extremes for each of eight phases of BSISO1 (a - h) from APHRODITE (color shading) and rain-gauge datasets (circle). Dots and filled circles indicate values that are significant at the 95% confidence level.

190x190mm (300 x 300 DPI)

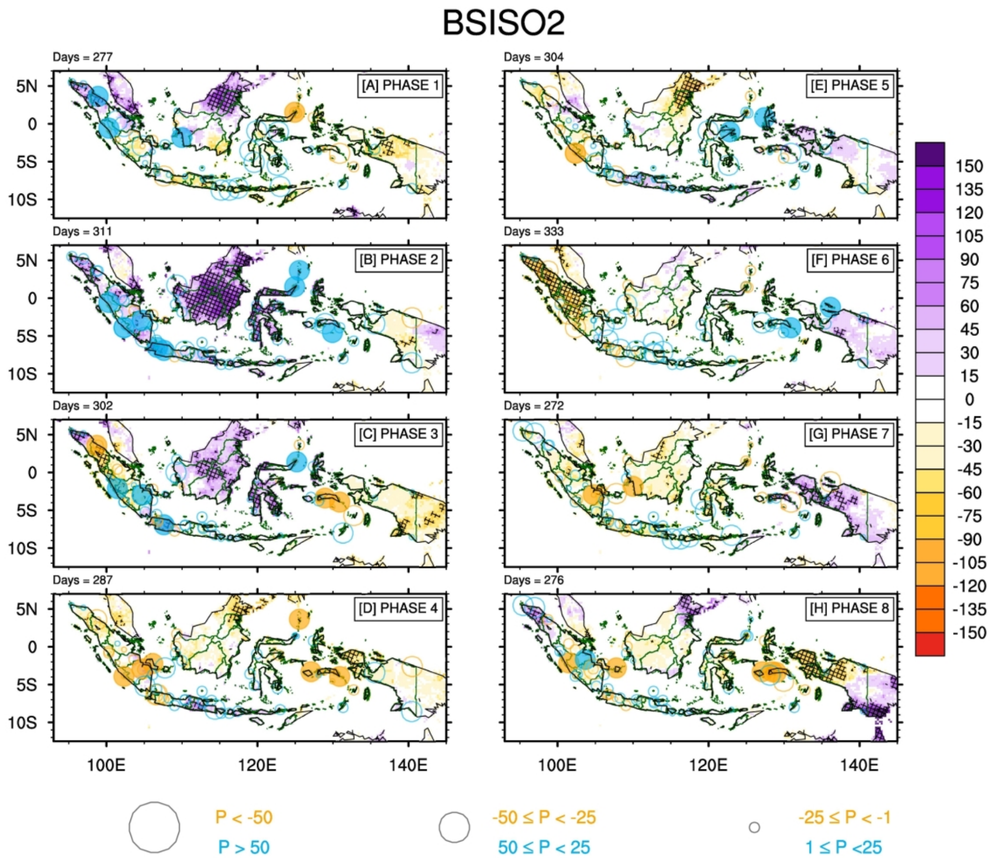

Figure 7. Same as Figure 6, but for BSISO2.

190x190mm (300 x 300 DPI)

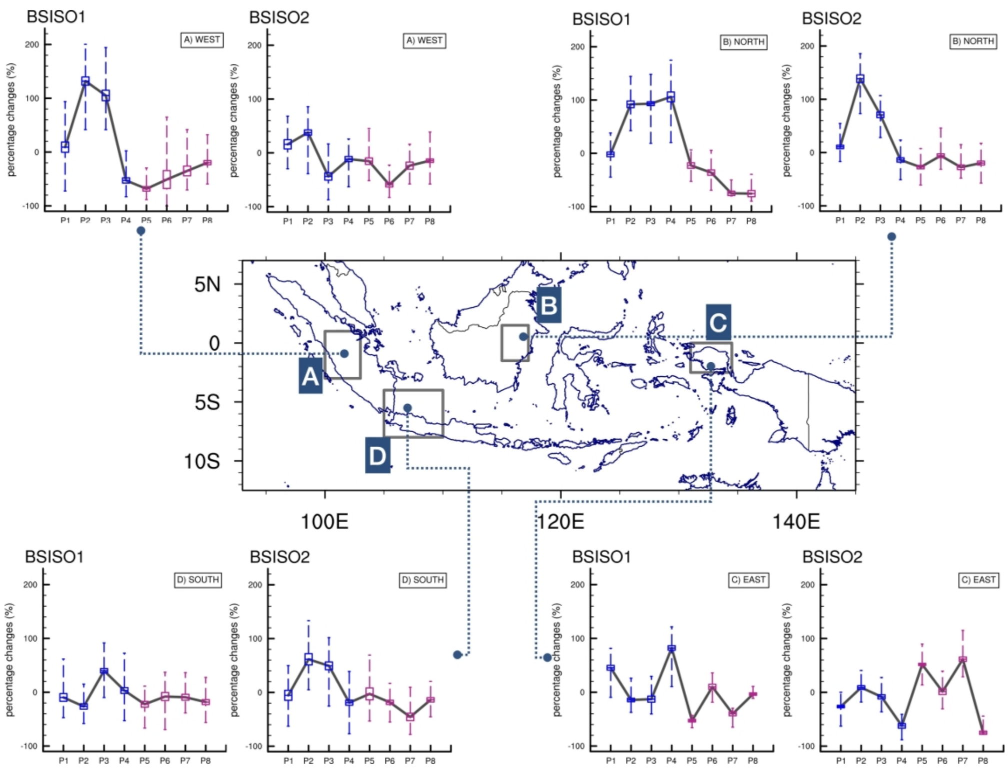

Figure 8. Percentage changes in the probability of extreme events based on APHRODITE data over the region of interest during different phases and types of BSISO. The upper and lower side of the box indicates the standard deviations, while the whiskers indicate the maximum and minimum values.

215x162mm (300 x 300 DPI)

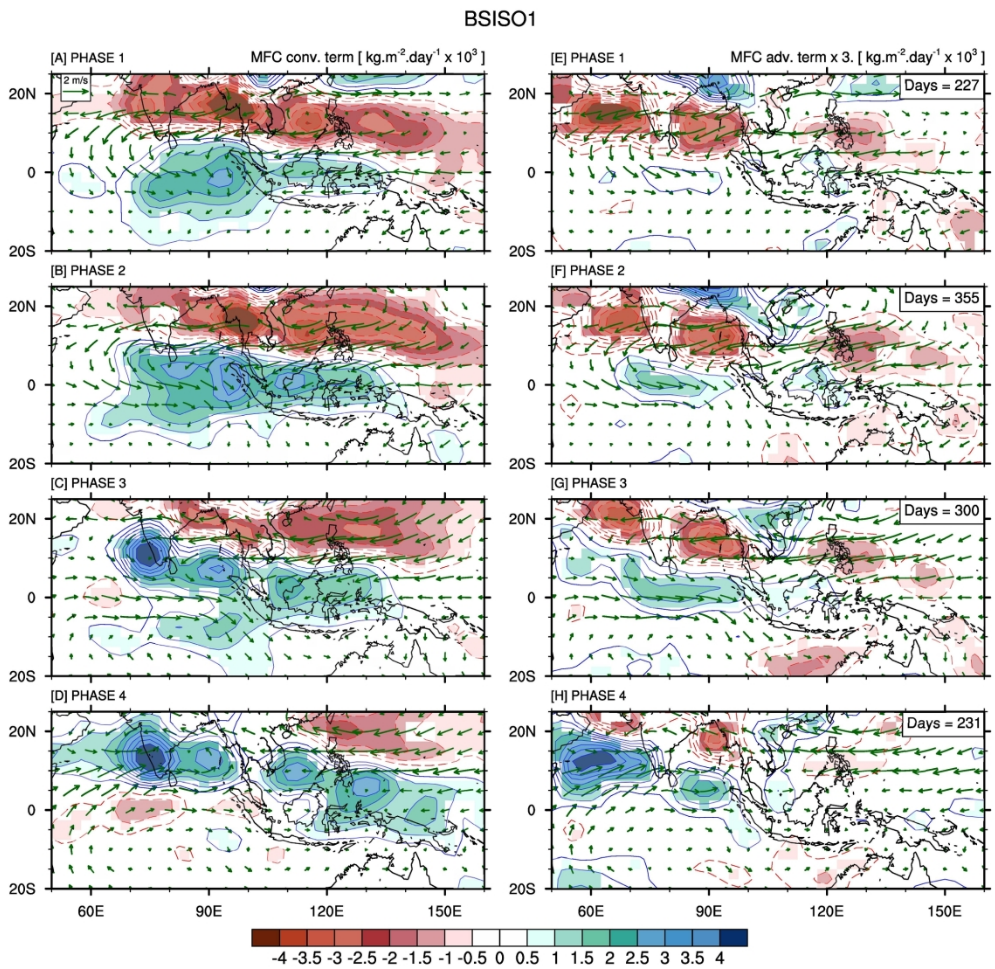

Figure 9. Life cycle composites of convergence term (a – d) and advective term (e – h) of MFC anomalies during phases 1 – 4 of BSISO1 (color shading) superimposed with 850-hPa wind (vector). Color shading indicates values significant at the 95% confidence level.

190x190mm (300 x 300 DPI)

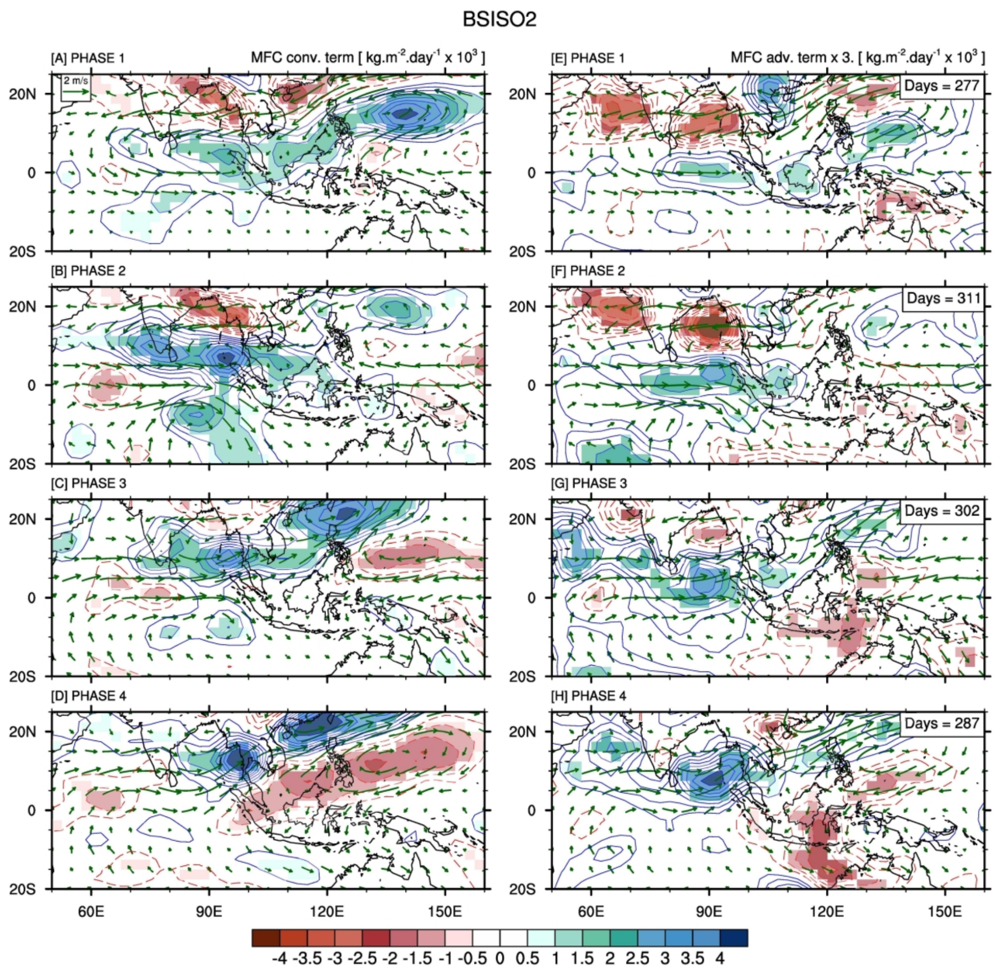

Figure 10. Same as Figure 9, except for BSISO2.

190x190mm (300 x 300 DPI)

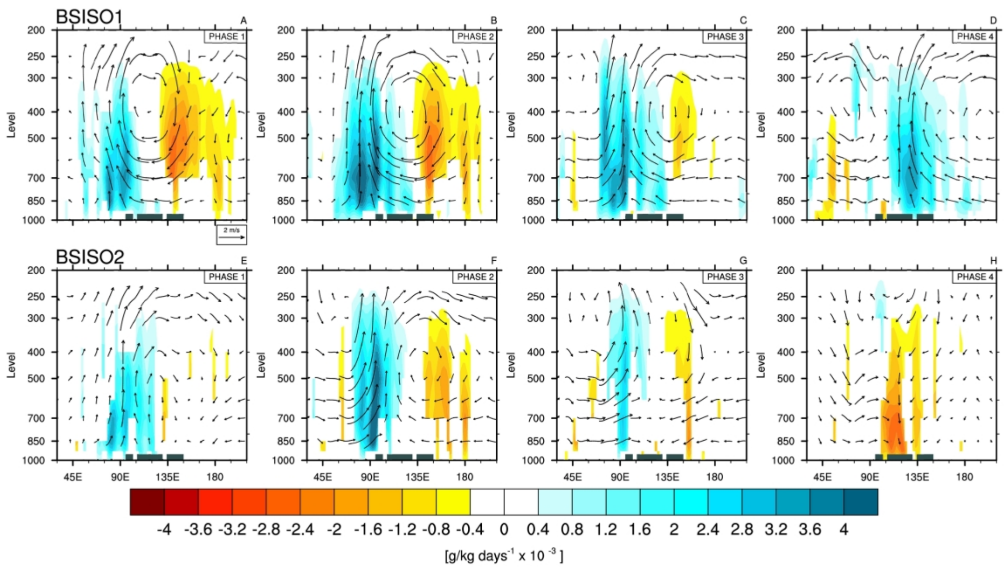

Figure 11. Zonal average (11^{o}S – 11^{o}N) of vertical moisture advection (color shading) during phases 1 - 4 of BSISO1 (a - d) and BSISO2 (e - h) superimposed with the zonal and vertical wind anomalies (vector). Color shading indicates values significant at the 95% confidence level.

254x215mm (300 x 300 DPI)

Table S1. The mean, 95th percentile, and percentage of missing data for each station. The stations are ordered from west to east. Underscored value denotes a station with more than 30% missing data and is omitted from the analysis (i.e., numbers 44, 60, and 62).

No	Latitude	Longitude	Miss	Mean	95th
1	5.52	95.42	10%	9.67	33.00
2	5.23	96.95	17%	11.41	46.00
3	3.62	98.71	6%	13.57	50.00
4	3.65	98.88	2%	13.84	50.50
5	-0.79	100.29	12%	20.37	74.90
6	-0.55	100.30	8%	22.73	87.48
7	0.46	101.45	12%	11.22	47.55
8	-2.08	101.45	7%	15.45	54.07
9	-3.87	102.31	7%	17.96	71.00
10	-0.33	102.32	23%	15.84	60.60
11	-3.86	102.34	10%	18.07	71.00
12	-3.55	102.59	12%	10.40	39.00
13	-1.63	103.64	6%	11.79	42.50
14	-2.89	104.70	11%	12.59	48.50
15	-2.93	104.77	11%	12.30	48.80
16	-5.16	105.11	6%	10.86	38.64
17	-3.65	106.11	10%	10.08	38.45
18	-2.17	106.13	12%	8.60	29.56
19	-6.29	106.56	12%	14.86	54.75
20	-5.52	106.65	4%	10.81	39.00
21	-6.50	106.75	11%	18.76	70.00
22	-6.26	106.75	9%	13.69	52.60
23	-6.88	107.60	8%	9.84	38.11
24	-2.75	107.75	5%	12.33	46.30

25	-6.73	108.26	1%	12.46	47.48
26	-7.72	109.01	11%	16.63	74.28
27	-0.79	109.12	7%	10.87	42.63
28	0.08	109.19	11%	16.51	66.12
29	1.74	109.30	5%	11.91	50.11
30	-1.80	109.97	7%	16.54	61.76
31	-6.98	110.38	13%	14.32	50.37
32	-6.95	110.42	1%	12.51	46.77
33	-5.85	112.66	17%	13.58	53.14
34	-7.21	112.74	6%	10.20	38.10
35	-7.38	112.78	8%	14.73	55.16
36	-7.04	113.91	6%	8.23	37.42
37	-8.22	114.36	13%	16.68	40.85
38	-8.75	115.17	8%	9.04	37.00
39	-8.75	116.25	10%	12.59	48.80
40	-8.49	117.41	4%	9.82	38.00
41	1.44	118.98	7%	11.45	43.14
42	-3.55	119.55	18%	11.59	44.70
43	-1.04	119.91	19%	9.46	35.00
<u>44</u>	<u>-0.92</u>	<u>122.62</u>	<u>60%</u>	<u>6.33</u>	<u>22.00</u>
45	-5.07	122.77	9%	11.32	44.00
46	-8.28	123.00	8%	8.37	40.54
47	3.69	124.92	6%	14.96	52.00
48	1.55	124.92	18%	13.57	49.95
49	1.55	125.18	14%	15.17	50.00
50	-5.47	125.53	11%	11.93	43.75
51	-5.66	127.08	9%	11.66	47.97

52	-3.25	127.38	13%	16.74	63.70
53	-3.88	128.10	10%	13.75	56.00
54	-3.25	128.40	11%	10.72	44.00
55	-3.71	128.93	5%	24.44	96.75
56	0.83	129.90	15%	14.26	55.00
57	-7.98	130.88	5%	10.61	41.53
58	-4.52	131.30	26%	13.50	57.00
59	-3.35	132.74	13%	20.48	81.15
60	-3.35	135.52	33%	17.93	68.50
61	-1.19	136.10	17%	13.55	45.87
62	-8.52	140.42	74%	7.19	29.94
63	-2.57	140.48	15%	9.30	37.52

4

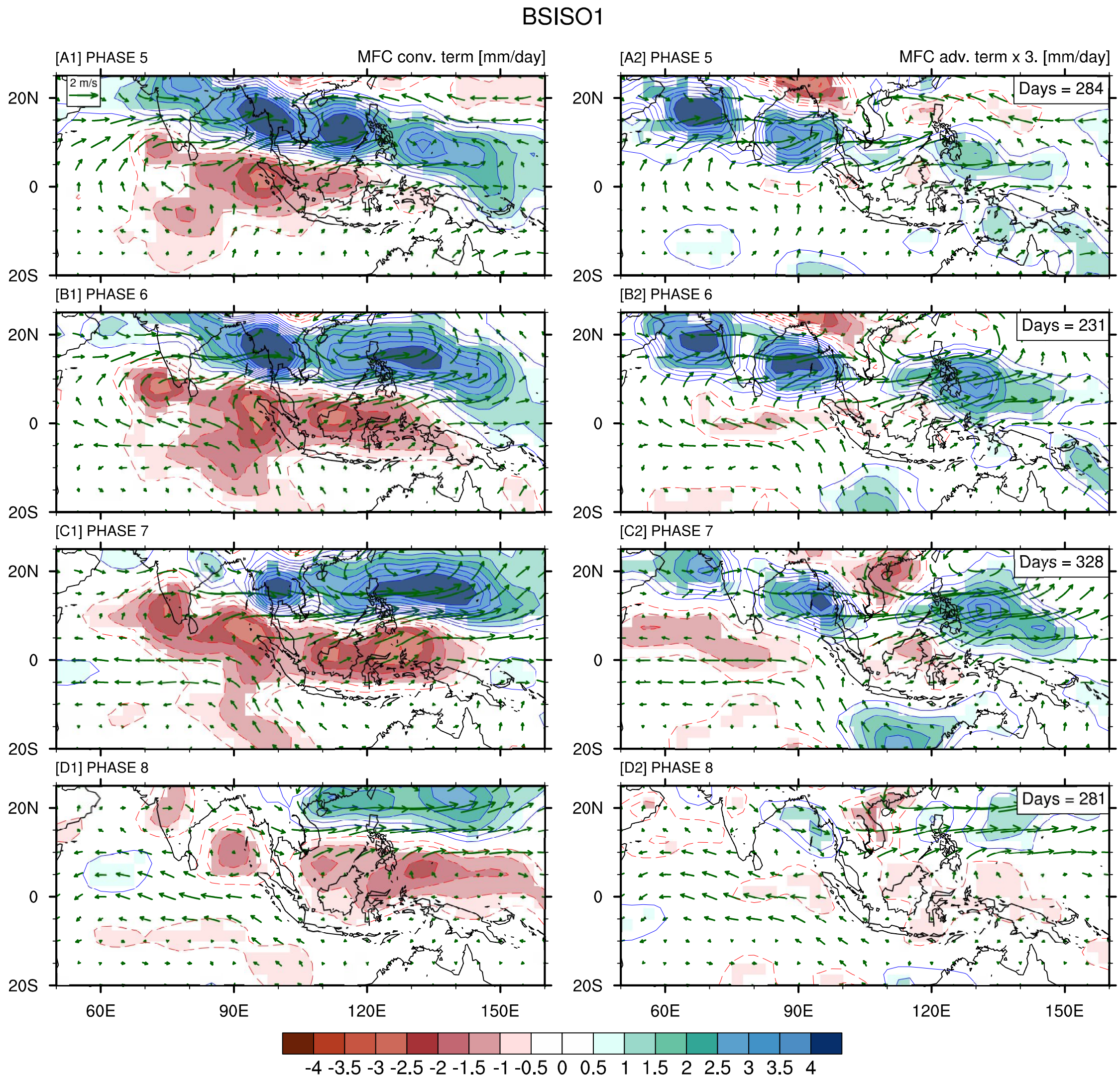

Figure S1. Life cycle composites of convergence term (a – d) and advective term (e – h) of MFC anomalies during phases 5 – 8 of BSISO1 (color shading) superimposed with 850-hPa wind (vector). Color shading indicates values significant at the 95% confidence level.

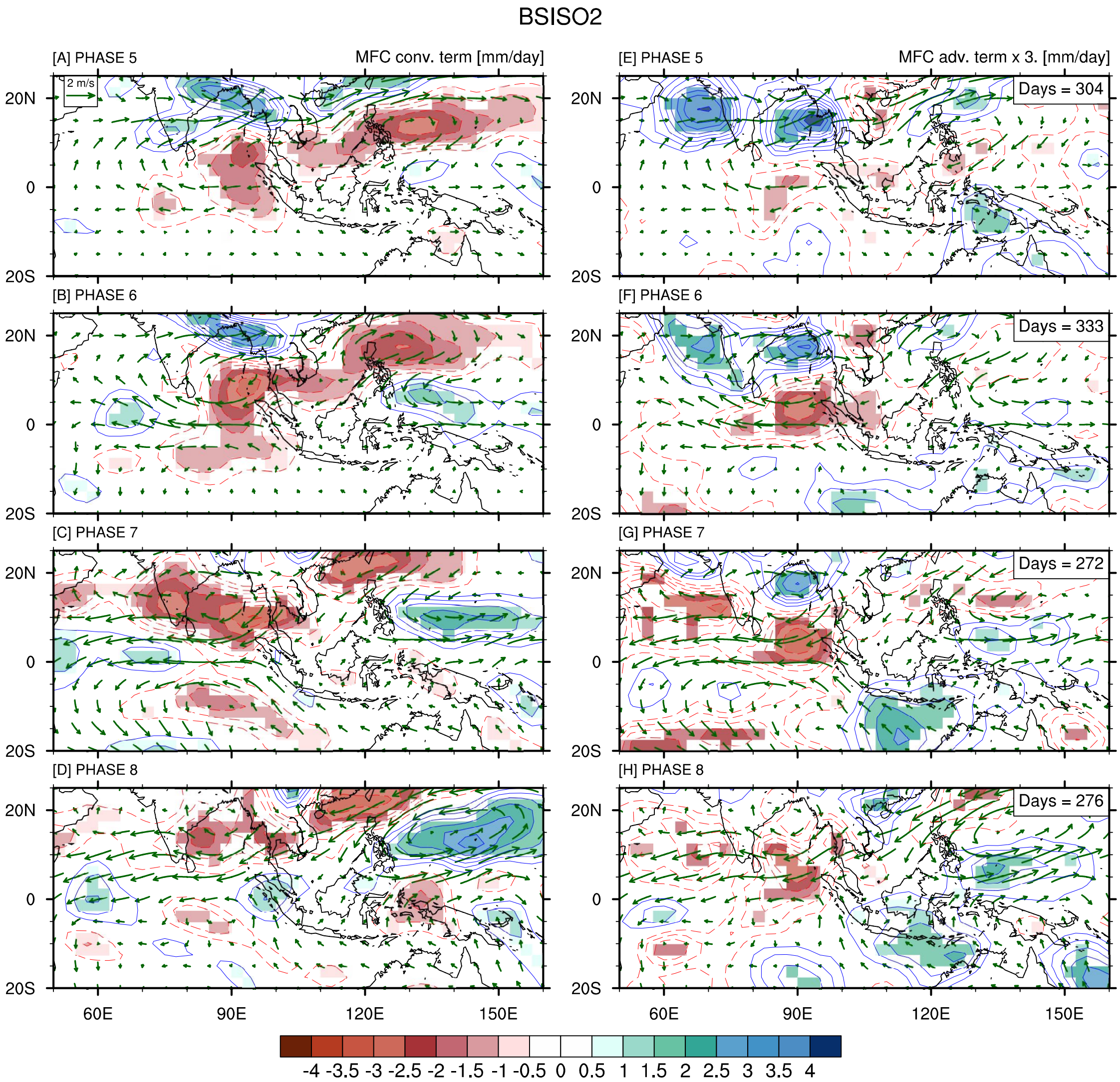

Figure S2. Life cycle composites of convergence term (a – d) and advective term (e – h) of MFC anomalies during phases 5 – 8 of BSISO2 (color shading) superimposed with 850-hPa wind (vector). Color shading indicates values significant at the 95% confidence level.

Impacts of the Boreal Summer Intraseasonal Oscillation (BSISO) on Precipitation Extremes in Indonesia

Fadhlil R. Muhammad* and Sandro W. Lubis

Impacts of BSISO on extreme precipitation events in Indonesia during extended boreal summer (May to August) are examined. The results indicate that under the influences of BSISO1, the probability of the rainfall extremes increases by 20 - 120% during phases 1 to 3 over Sumatra and Borneo. Under the BSISO2, the probability of the extremes increases up to 40% over Sumatra during phases 1 to 2 and up to 140% over the Borneo and Sulawesi during phases 2 - 3. The changes in the probability are found to be associated with BSISO-induced moisture flux convergence and vertical advection of moisture.

Percentage changes in extreme precipitation probability associated with BSISO